PAPER

Check for updates

Enhanced dye removal and supercapacitor performance of polyethyleneimine-impregnated activated carbon derived from local eucalyptus biochar

Bordin Weerasuk, Threeraphat Chutimasakul, Nicha Prigyai and Tanagorn Sangtawesin [ID] *

This study evaluated the effectiveness of low-cost eucalyptus biochar (EUBC) as a precursor for activated carbon (EUAC), for methyl orange (MO) removal and supercapacitor applications. The surface charge was made positive by impregnating EUAC with a 10% weight polyethyleneimine (PEI) solution, improving anionic MO adsorption. The impregnation was verified by SEM and XPS, showing a nitrogen content of 9.39%. The adsorption capacity of the 10% wt PEI/EUAC is 142 mg g^{-1}, significantly surpassing previous reports. The adsorption mechanisms were described using the Sips isotherm and Elovich kinetics, indicating heterogeneous adsorption, physisorption and electrostatic interactions. In electrochemical tests, EUAC (263 F g^{-1}) and 10% wt PEI/EUAC (244 F g^{-1}) exhibited similar specific capacitances, six times higher than that of EUBC (40 F g^{-1}) at a current density of 1 A g^{-1}. However, EUBC electrodes exhibited nearly double the internal resistivity of those from EUAC and 10% wt PEI/EUAC, attributed to particle size, pore size, and surface area differences.

Sustainability spotlight

This study enhances the sustainability of dye removal and energy storage processes by utilizing locally sourced eucalyptus biochar, modified with polyethyleneimine (PEI). This innovation not only improves the biochar's effectiveness in removing harmful methyl orange dye from water, but also bolsters its utility in supercapacitors. By using local resources and creating reusable activated carbon, we significantly reduce the environmental impact associated with material transportation and waste, directly supporting SDG 6 (Clean Water and Sanitation) and SDG 7 (Affordable and Clean Energy). This dual functionality showcases a scalable, sustainable solution to critical environmental and energy challenges.

1 Introduction

Water pollution from the textile industries poses a significant threat to the global aquatic environment, ecosystem sustainability, and human health due to the introduction of harmful substances and disruption of natural processes.[1–4] Approximately 140 000 tons of azo dyes, recognized for their toxicity and carcinogenic properties, are released into aquatic systems annually, adversely affecting human health and ecosystem integrity.[5–7] Methyl orange (a common anionic dye in textile industries) can cause mutagenic changes under oxidative conditions, potentially forming carcinogenic anilines or reactive oxygen species. This breakdown can be further catalyzed by specific bacteria and enzymes, emphasizing the need for its removal from water bodies. In this context, adsorption emerges as a particularly effective method for extracting methyl orange

from aqueous environments due to its efficiency, cost-effectiveness, and simplicity.[8–10]

Activated carbon is increasingly recognized for its potential in pollution treatment due to its renewable, sustainable, and cost-effective nature and extensive surface area and high porosity.[11–13] Eucalyptus has been identified as a viable carbon source for producing biochar and activated carbon. The price of local-enterprise eucalyptus biochar in Thailand is about 0.25 USD per kg. However, if the adsorption ability increases, the price significantly increases 50–200%. Anastopoulos' review of activated carbon derived from eucalyptus highlighted its efficacy in heavy-metal adsorbents, demonstrating superior performance in this domain. Furthermore, this material has shown promise in the adsorption of various dyes, including malachite green (MG), methylene blue (MB), Congo red (CR), Eriochrome Black T (EBT), methyl violet (MV), Basic Red 12 (BR12), Basic Blue 41 (BB41), crystal violet (CV), Solar Red (SR), Brittle Blue (BB), and indigo carmine (IC).[14] However, only a few studies have explored the adsorption capabilities of eucalyptus-derived activated carbon or biochar specifically for anionic

Thailand Institute of Nuclear Technology (Public Organization), 9/9 Moo 7, Saimoon, Ongkharak, Nakhon Nayok 26120, Thailand. E-mail: tanagorn@tint.or.th

methyl orange (MO), which causes eye irritation and gastrointestinal tract irritation.[15] Enhancing activated carbon's adsorption capacity for specific adsorbates can be achieved through various methods, such as plasma treatment, thermal treatment, and chemical impregnation. These techniques are designed to increase the presence of active functional groups and the ion exchange capacity of the activated carbon, thereby improving its efficiency in pollutant removal.[16,17]

Polyethyleneimine (PEI), a water-soluble polymer endowed with amine functional groups, exhibits significant selectivity for anionic dyes due to electrostatic interactions.[18–20] Moreover, PEI is advantageous for its cost-effectiveness, non-toxic nature, and excellent biocompatibility.[21] However, as PEI is water-soluble, it requires a solid support to enhance its stability and facilitate its use in adsorption applications. Recently, Liu *et al.* reported corncob-derived activated carbon modified with PEI for MO dye and Cr(VI) removal and achieved 100% and 95% removal, respectively.[21] Wong *et al.* modified activated carbon from spent tea leaves with PEI for MO removal at 62.11 mg g^{-1}.[22] Mohamed *et al.* studied the adsorption of MO dye (80% removal) using activated carbon derived from sugarcane bagasse.[23] Thus, modification of activated carbon with PEI is an alternative method to increase the MO adsorption capacity.

Incorporating nitrogen functional groups into activated carbon has been shown to enhance its hydrophilic properties, capacitance, and electrical conductivity, all of which are crucial for electrode materials in energy storage applications. PEI-based nitrogen-doped carbon nanofibers were designed specifically for supercapacitor electrodes, exhibiting a noteworthy specific capacitance of 200 F g^{-1} at a current density of 1 A g^{-1}, with a capacitance retention of 84.25%, even at an increased current density of 10 A g^{-1}.[24] Similarly, nitrogen-doped activated carbon using PEI approached high specific capacitance values of 268 F g^{-1} in acidic electrolytes and 226 F g^{-1} in organic electrolytes at a scan rate of 1 mV s^{-1}.[25] These materials also demonstrated exceptional durability, maintaining 95.5% of their capacitance after 15 000 charge–discharge cycles at 20 A g^{-1}.[25] These findings underscore the effectiveness of nitrogen doping in enhancing the performance of carbon-based electrodes for supercapacitors.

Herein, this research investigated the effect of PEI impregnation on activated carbon derived from local-enterprise eucalyptus biochar. The physico-chemical properties, methyl orange adsorption properties and electrochemical properties were studied. Unlike previous studies, which typically started by producing activated carbon or biochar from biomass, this approach emphasizes utilizing biochar made by local producers and enhancing local profits.

2 Experimental

2.1 Preparation of biochar

Eucalyptus biochar (EUBC) was obtained from a community enterprise in Ongkharak District, Nakhon Nayok Province, Thailand. The EUBC was crushed with a high-speed crusher and passed through a 200-mesh sieve.

2.2 Preparation of activated carbon

A 1 : 2 weight ratio of biochar and KOH was used. Briefly, 5 g of EUBC was mixed with 10 g of KOH (AR grade, purchased from KEMAUS Ltd, Australia). Then, the sample was activated at 800 °C for 5 hours in a tube furnace (TMAX Furnace TL1200) with N$_2$ gas. After that, the activated carbon (AC) was taken out of the furnace and rinsed with 0.1 M H$_2$SO$_4$ (AR, RCI Labscan Ltd, EN), followed by washing with distilled water (18.2 MΩ cm resistivity) until pH 7 was reached. Finally, the AC sample was dried at 60 °C for 24 hours and labeled as EUAC.

2.3 Modification of activated carbon with polyethyleneimine

Fig. 1 shows a diagram of the sample preparation. 10 wt% PEI (PEI, AR grade, Sigma-Aldrich) was dissolved in 10 mL of ethanol (C$_2$H$_5$OH, 99.9% AR grade, RCI Labscan) and stirred for 30 minutes. Then, 1.2 g of EUAC was added to the PEI solution. The solution was stirred until the ethanol was completely evaporated. Next, the sample was dried in an oven at 60 °C for 12 hours to obtain PEI/EUAC adsorbent with a PEI loading of 10 wt%, marked as 10% wt PEI/EUAC.

2.4 Physical and chemical characterization

The morphology of the EUAC samples was characterized *via* scanning electron microscopy (SEM, SU5000 Hitachi). The surface area and N$_2$ adsorption–desorption isotherm were analyzed using a surface area and porosity analyzer (BET, ASAP2460, Micromeritics). Raman spectroscopy at a 532 nm laser wavelength (XploRA™ PLUS, Horiba) was used to investigate the graphitic content. X-ray photoelectron spectroscopy (XPS, AXIS Ultra DLD, Shimadzu) was used to identify elemental components and chemical structure.

2.5 Dye adsorption experiment

Methyl orange (MO), an anionic dye with the chemical formula of C$_{14}$H$_{14}$N$_3$NaO$_3$S and a molecular weight of 327.33 g mol^{-1}, was purchased from Sigma-Aldrich. To study the MO adsorption efficiency, 20 mg of EUAC or PEI/EUAC was added to 40 mL of MO (75 ppm). Then, the mixture was shaken at 150 rpm at 30 °C for 6 h. The solution was filtered through a syringe filter
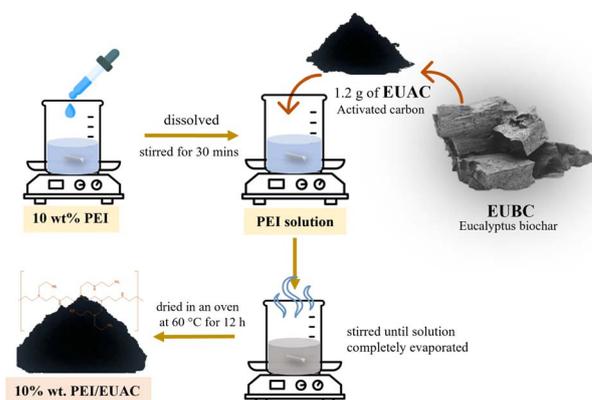

Fig. 1 Sample preparation.

(0.45 micron pore diameter) and the remaining concentration of MO was analyzed by using a UV-Vis spectrophotometer at 474 nm. The adsorption capacity (q_e, mg g^{-1}) and the removal percentages of MO dye (% R) were calculated according to the MO concentration before and after adsorption, as shown in eqn (1) and (2), respectively.

$$q_e = \left(\frac{C_0 - C_e}{m}\right)V \quad (1)$$

$$\% R = \left(\frac{C_0 - C_e}{C_0}\right) \times 100 \quad (2)$$

where q_e is the quantity of adsorbate per unit mass of adsorbent (mg g^{-1}), C_0 is the initial MO concentration (mg L^{-1}), C_e is the MO concentration at equilibrium (mg L^{-1}), m is the amount of adsorbent (g), and V is the volume of the diluent (L).

Furthermore, the adsorption isotherm was investigated and fitted with Langmuir (eqn (3)), Freundlich (eqn (4)), Sips (eqn (5)), and Temkin (eqn (6)) models.[26,27]

Langmuir:

$$q_e = q_{max}K_L C_e/(1 + K_L C_e) \quad (3)$$

Freundlich:

$$q_e = K_F(C_e^{1/n}) \quad (4)$$

Sips:

$$q_e = q_s K_s C_e^n/(1 + (K_s C_e^1)) \quad (5)$$

Temkin:

$$q_e = B \ln(K_T C_e) \quad (6)$$

Here, q_{max} (mg g^{-1}) is the Langmuir maximum adsorption capacity, and K_L (L mg^{-1}) is the Langmuir adsorption coefficient. K_F (mg$^{(1-1/n)}$ g^{-1} L$^{1/n}$) is Freundlich affinity, and n is the Freundlich empirical constant. K_s (L mg^{-1}) is the coefficient related to the Sips model. q_s is the Sips adsorption capacity (mg g^{-1}), and n is the Sips isotherm model exponent. In addition, K_T (L mg^{-1}) and B (mg g^{-1}) are the Temkin model constants.

The adsorption kinetics were studied at predetermined time intervals over 6 hours and fitted with pseudo-first-order (eqn (7)), pseudo-second-order (eqn (8)), and Elovich (eqn (9)) equations.[26,27]

Pseudo-first-order:

$$q_t = q_e(1 - e^{-K_1 t}) \quad (7)$$

Pseudo-second-order:

$$q_t = (K_2 q_e^2 t)/(1 + K_2 q_e t) \quad (8)$$

Elovich:

$$q_t = (1/\alpha)\ln(1 + \alpha\beta t) \quad (9)$$

Notably, q_t is the amount of MO at t minutes (mg g^{-1}), while K_1 and K_2 are the rate constants for the pseudo-first-order

(min^{-1}) and second-order (g mg^{-1} min^{-1}) models, respectively. Meanwhile, α is the initial adsorption rate for the Elovich model (mg g^{-1} min^{-1}) and β is the desorption constant (g mg^{-1}).

2.6 Reusability study

In each cycle, the procedure of the reusability test was carried out with the same conditions as the absorption experiment. Before running the next cycle, the adsorbent was washed three times with 10 mL of deionized water, followed by centrifuging at 4500 rpm for 10 min, and the adsorbent was dried in an oven at 55 °C for 2 hours. The removal efficiency of MO over the studied adsorbent was determined in each cycle to evaluate the reusability.

2.7 Fabrication of supercapacitor electrode and electrochemical measurements

The working electrode was prepared from graphite foil coated with a mixture of 5% w/v polyvinylidene fluoride (PVDF) dispersed in N-methyl-2-pyrrolidone (NMP), carbon black (Alfa Aesar) additive and the synthesized activated carbon (10% wt PEI/EUAC). Briefly, the mixture was prepared by ultrasonically mixing 5% w/v PVDF in NMP, carbon black powder and 10% wt PEI/EUAC in a weight ratio of 1 : 1 : 8 for 30 minutes. The mixture was drop-casted on a graphite foil electrode with an active surface area of 2 × 2 cm^2. The coated electrode was dried in an oven for approximately 24 hours at 100 °C. The total active mass loading in each electrode was approximately 4–5 mg.

The electrochemical performances were determined by using cyclic voltammetry (CV), galvanostatic charge/discharge (GCD) and electrochemical impudence spectroscopy (EIS) measurements. A regular three-electrode system (Potentiostat Plamsens 4) was used in this work. The synthesized activated carbon coated on a graphite foil electrode, Pt wire and Ag/AgCl (ItalSens) were used as the working, counter and reference electrodes, respectively. All experiments were conducted at room temperature under ambient conditions with 2 M H$_2$SO$_4$ electrolyte. The cyclic voltammograms were recorded at different scan rates of 10 to 50 mV s^{-1}. The galvanostatic charge/discharge curves were recorded at different current densities from 1 to 5 A g^{-1}. The EIS measurements were tested in the frequency range of 10 kHz to 1 Hz. The impedance was reported in the form of Nyquist plots (real impedance Z' as a function of the imaginary one Z'').

3 Results and discussion

3.1 Characterization of biochar and activated carbon

The SEM images of EUAC and 10% wt PEI/EUAC are shown in Fig. 2. EUAC showed a smooth surface (Fig. 2a–c), while the morphological structure of 10% wt PEI/EUAC (Fig. 2d–f) presented a relatively smooth surface with the presence of spherical particles on the surface. These particles were extensively coated on the surface of 10% wt PEI/EUAC, which indicated the aggregation and layer coating of PEI. This result confirms that the EUAC surface was successfully impregnated with PEI.
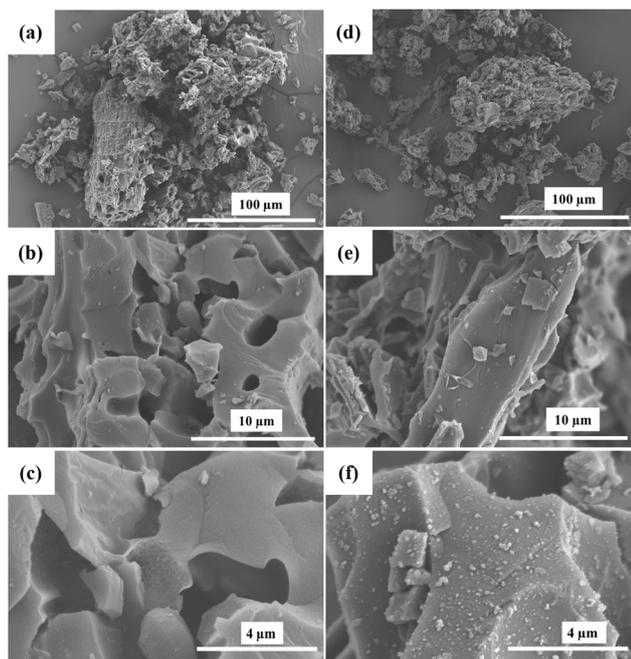
Fig. 2 SEM images of (a–c) EUAC and (d–f) 10% wt PEI/EUAC at magnifications of ×100, ×3.5k and ×12k, respectively.

Raman spectroscopy was used to evaluate the degree of graphitization in the carbon materials. The Raman spectra of EUBC, EUAC and 10% wt PEI/EUAC are shown in Fig. 3. The peak around 1344 cm^{-1} corresponds to the sp^3-hybridization of the carbon atoms (D-band), indicating a disordered and amorphous structure. The second peak around 1584 cm^{-1} relates to the sp^2-hybridized carbon atoms in the material (G-band), which demonstrates the crystalline graphitic structure. The ratio of the D/G band intensity (I_D/I_G) reveals the degree of graphitization, in other words the level of disorder/order in carbon materials. The I_D/I_G ratios of EUBC and EUAC are 0.71 and 0.94, respectively. After modification of activated carbon with PEI, the ratio value of I_D/I_G for 10% wt PEI/EUAC is 0.99, which may result in an irregular configuration of the carbon atoms, corresponding to a previous report.[24]
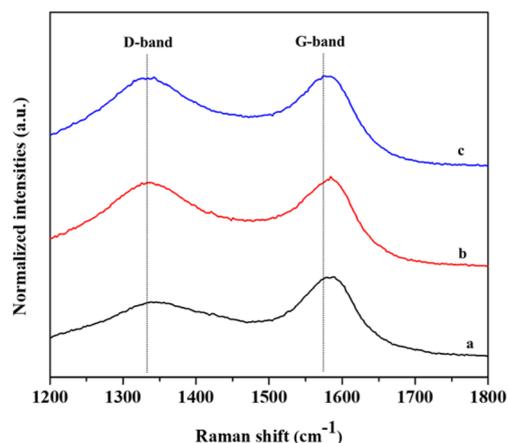

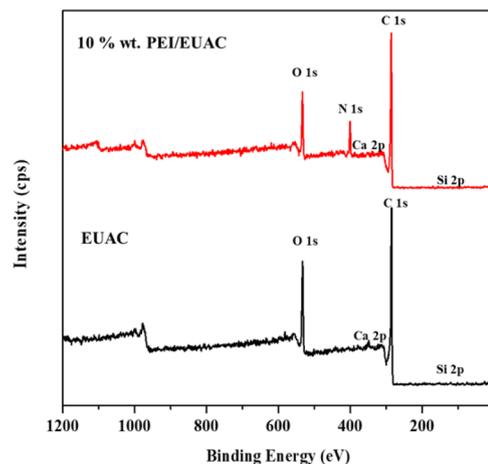Fig. 3 Raman spectra of (a) EUBC, (b) EUAC and (c) 10% wt PEI/EUAC.

Fig. 4 XPS survey spectra of EUAC and 10% wt PEI/EUAC.

The elemental components were analyzed by using the X-ray photoelectron spectroscopy (XPS) technique. Fig. 4 shows the XPS survey spectrum of EUAC, revealing the carbon and oxygen peaks at 285 eV (C 1s) and 533 eV (O 1s), respectively. For 10% wt PEI/EUAC, a nitrogen peak appeared at 400 eV, indicating PEI on the AC's surface, and this result is in good agreement with the SEM analysis. The high-resolution XPS spectra of EUAC are shown in Fig. 5a and b. The C 1s profile of EUAC was found to exhibit six fitted peaks, including C–Si (283.96 eV), C–C (283.9 eV), C–OH (285.8 eV), C=O (286.91 eV), O–C=O (288.1 eV) and COOH/COOR (289.2 eV).[28,29] The O 1s spectrum of EUAC exhibited four peaks at C–OH (531.3 eV), C=O/C–O–C (532.3 eV), O=C–O (533.5 eV) and chemisobed oxygen and/or water (534.5 eV), as shown in Fig. 5b.

For 10% wt PEI/EUAC (Fig. 5c–e), the material mainly consisted of carbon, oxygen and nitrogen, where the nitrogen was obtained from PEI. The C 1s spectrum of 10% wt PEI/EUAC was composed of five fitted peaks: C–C (284.96 eV); C–O (286.17 eV); C=O (286.9 eV), O–C=O (288.6 eV) and COOH/COOR (289.9 eV) as shown in Fig. 5c. The O 1s XPS spectrum (Fig. 5d) also consists of four peaks, the same as those presented for EUAC. In addition, the N 1s spectrum of 10% wt PEI/AC exhibited three fitted peaks: pyrrole (400.14 eV), graphitic-N (401.22 eV) and quaternary-N (402.2 eV),[30–32] as shown in Fig. 5e. The XPS analysis of 10% wt PEI/EUAC demonstrated that the EUAC surface was successfully impregnated with PEI. Moreover, the relative atomic concentrations of C, O, and N from XPS analysis are presented in Table 1. 10% wt PEI/EUAC was found to contain 9.39% nitrogen, which indicates the presence of PEI in this material.

The specific surface area (SA) and porosity of EUBC, EUAC and 10% wt PEI/EUAC were analyzed using N$_2$ adsorption–desorption isotherms. The specific surface areas (SAs) of EUBC, EUAC and 10% wt PEI/EUAC were acquired using the Brunauer–Emmett–Teller (BET) method and are summarized in Table 2. The N$_2$ adsorption–desorption isotherm for EUBC can be classified as type I (Fig. 6); this isotherm is parallel over the relative pressure range, which corresponds to a micropore structure
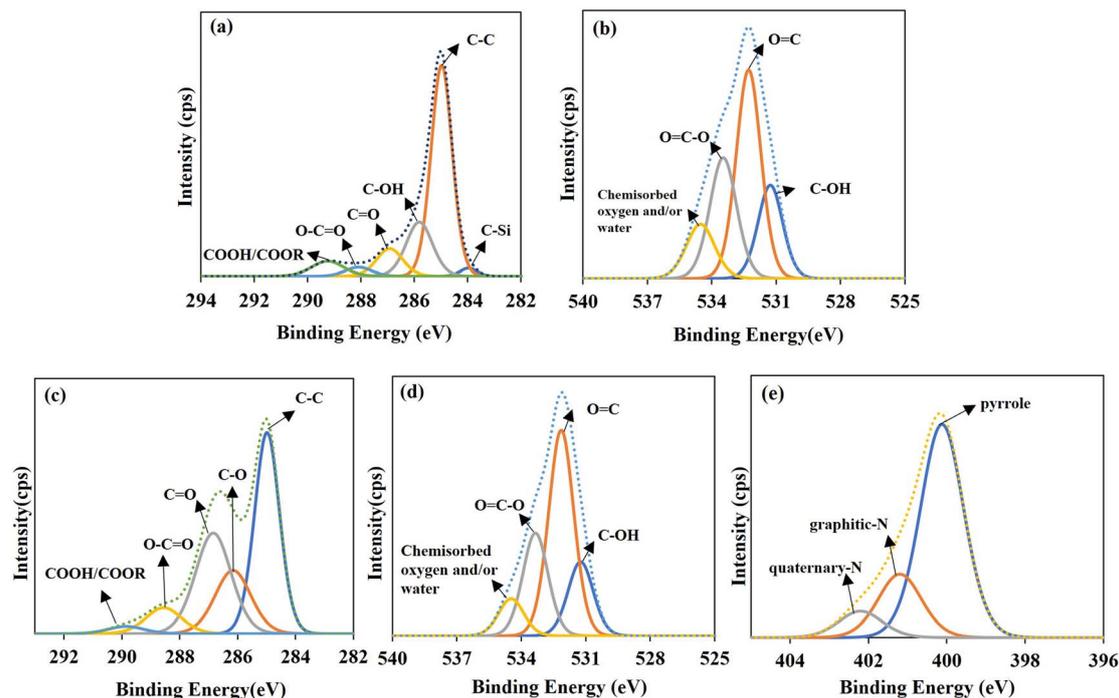
Fig. 5 (a) C 1s and (b) O 1s XPS spectra of EUAC as well as (c) C 1s, (d) O 1s and (e) N 1s of 10% wt PEI/EUAC.

Table 1 The chemical compositions of EUAC and 10% wt PEI/EUAC were determined using the XPS technique

Sample	Atomic percent (%)					
	C_{1s}	O_{1s}	Ca_{2p}	Si_{2p}	Al_{2p}	N_{1s}
EUAC	25.27	12.79	0.50	0.73	0.72	—
10% wt PEI/EUAC	78.25	11.99	0.36	6.36	—	9.39

with monolayer adsorption.[26,27] However, the isotherms of EUAC and 10% wt PEI/EUAC can be classified as type IV isotherms with an H4-type hysteresis loop (Fig. 6), indicating the existence of micro- and mesopores and reflecting multilayer adsorption on the surface.[26,27] In addition, the specific surface areas of EUBC, EUAC and 10% wt PEI/EUAC are 143.70, 1150.15 and 1154.61 $m^2 g^{-1}$, respectively (Table 2). Likewise, a micropore volume of 0.06 $cm^3 g^{-1}$ was found in EUBC, while 0.49 $cm^3 g^{-1}$ was found in 10% wt PEI/EUAC and EUAC.

The zeta potentials of the samples were tested by using a Malvern Zetasizer Ultra. The zeta potential of the EUAC surface in aqueous solution was −29.5 mV. After impregnation with PEI, the zeta potential of 10% wt PEI/EUAC increased to +47.8 mV

because the amine groups of PEI (–NH or NH_2) could readily adsorb cations (H^+) and exhibit a positive charge on the surface.

3.2 Methyl orange adsorption

Fig. 7 shows the MO adsorption capacity (q_e, mg g^{-1}) of EUBC, EUAC and 10% wt PEI/EUAC at contact times of 1–6 hours. The q_e of EUBC, EUAC and 10% wt PEI/EUAC increased rapidly and then reached an equilibrium stage at 6 hours. The q_e values of EUBC, EUAC and 10% wt PEI/EUAC at a contact time of 6 hours were 4.13, 79.73 and 141.65 mg g^{-1}, respectively. With 10 wt% PEI, there were more surface adsorption sites and a higher surface area, and thus a better ability for MO capture. 10% wt PEI/EUAC (94.43%) exhibited higher removal efficiency than EUBC (2.75%) and EUAC (79.73%). Therefore, only 10% wt PEI/EUAC was selected for further investigating the adsorption isotherm and kinetics.

3.3 Adsorption isotherm

This experiment used 10% wt PEI/EUAC and MO solution at a ratio of 10 mg : 40 mL with the same procedure as mentioned in the Experimental part. With these conditions, the q_e of

Table 2 Surface properties of EUBC, EUAC, and 10% wt PEI/EUAC

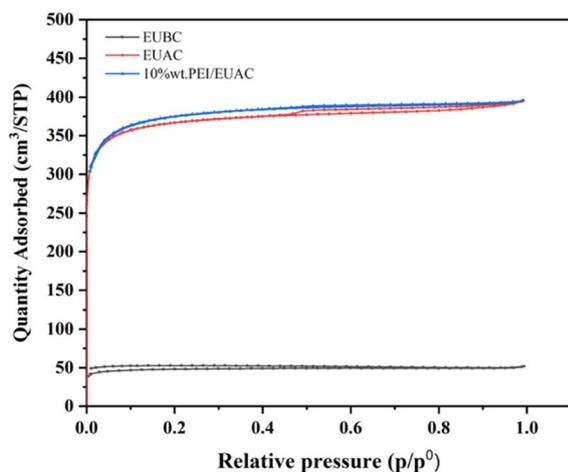| Samples	BET SA ($m^2 g^{-1}$)	A_{micro} ($m^2 g^{-1}$)	A_{meso} ($m^2 g^{-1}$)	V_{total} ($cm^3 g^{-1}$)	V_{micro} ($cm^3 g^{-1}$)	V_{meso} ($cm^3 g^{-1}$)	Avg. pore size (nm)
EUBC	143.70	121.61	13.42	0.07	0.06	0.01	2.78
EUAC	1150.15	975.63	105.29	0.60	0.49	0.11	3.05
10% wt PEI/EUAC	1154.61	946.00	208.60	0.61	0.49	0.12	2.59

Fig. 6 N$_2$ adsorption–desorption isotherms of the EU series.

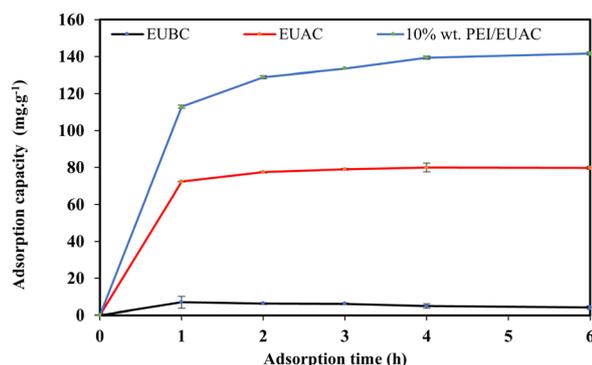**Fig. 7** The MO adsorption capacities (75 ppm) of EUBC, EUAC and 10% wt PEI/EUAC.

10% wt PEI/EUAC increased to 385.5 mg g^{-1}. The adsorption isotherm experiments were performed at initial MO concentrations of 25–200 ppm and fitted with the Langmuir, Freundlich, Temkin, and Sips isotherm models,[33–35] as shown in Fig. 8. The Sips model's correlation coefficient (R^2) was 0.99419, considerably higher than those of the other models (Table 3). The results suggested that the adsorption process of MO with 10% wt PEI/EUAC is better fitted with the Sips model, which demonstrates a mixture of behaviors of the Langmuir and Freundlich isotherms. The Sips isotherm model asserts that the adsorption process obeys the Freundlich isotherm at a lower concentration, followed by the Langmuir isotherm at a high concentration. The mechanism of MO adsorption on 10% wt PEI/EUAC would be a combination of electrostatic attraction and physisorption.

3.4 Adsorption kinetics

The relationship between an adsorbent's adsorption capacity and contact time is commonly analyzed through adsorption kinetics models. In this context, pseudo-first-order, pseudo-second-order, and Elovich kinetic models were applied to interpret the experimental data presented in Fig. 9. The
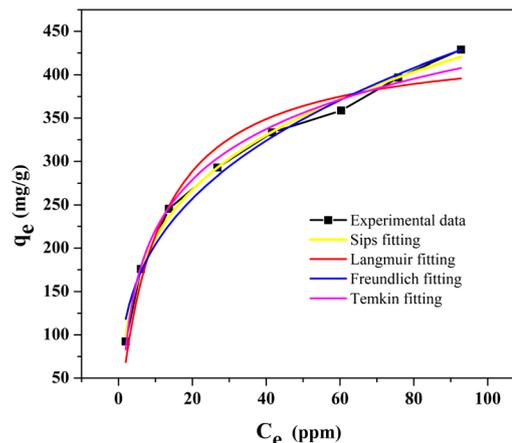

Fig. 8 Langmuir, Freundlich, Sips, and Temkin isotherm fits of the experimental MO adsorption equilibrium data (150 ppm) by 10% wt PEI/EUAC, where C_e (mg L^{-1}) is the equilibrium concentration of the adsorbate.

Table 3 Isotherm parameters for 10% wt PEI/EUAC

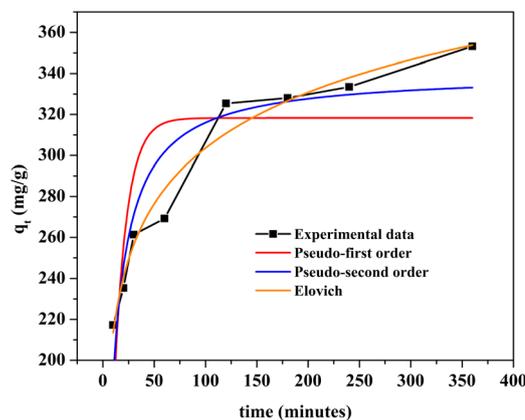| Model	Parameter	Sample
Langmuir	q_{max} (mg g^{-1})	440.90
	K_L (L mg^{-1})	0.0947
	R^2	0.96011
Freundlich	K_F (mg$^{1-1/n}$ g^{-1} L$^{1/n}$)	94.804
	n	3.002
	R^2	0.98301
Sips	q_s (mg g^{-1})	124.85
	K_s (L g^{-1})	1.0000
	n	1.2703
	R^2	0.99419
Temkin	B (J mol^{-1})	84.037
	K_T (L g^{-1})	1.3833
	R^2	0.98851

Fig. 9 Pseudo-first-order, pseudo-second-order and Elovich fits of the adsorption kinetics data for the MO adsorption (150 ppm) by 10% wt PEI/EUAC, where q_t is the adsorption capacity at time t (minutes).

correlation coefficient (R^2) associated with the Elovich model, which stood at 0.96721, surpassed that of the pseudo-first-order and second-order models (Table 4). Elovich's model is suitable

Table 4 Kinetic parameters for 10% wt PEI/EUAC

Model	Parameter	Sample
Pseudo-first-order	q_e (mg g^{-1})	318.26
	K_1 (min^{-1})	0.08139
	R^2	0.57205
Pseudo-second-order	q_e (mg g^{-1})	340.23
	K_2 (g (mg min)$^{-1}$)	5.14×10^6
	R^2	0.85070
Elovich	α (mg (g min)$^{-1}$)	902.92
	β (g mg^{-1})	0.0255
	R^2	0.96721

for heterogeneous surface adsorption. This model implies multilayer adsorption and assumes that the adsorption sites increase exponentially with adsorption.

From our previous studies,[36] the pH of the point of zero charge for eucalyptus-derived biochar (EUBC) and activated carbon (EUAC) ranges between 6.6–7.1. Consequently, their negatively charged surfaces are predisposed to adsorb cationic dyes rather than anionic dyes. However, following impregnation with polyethyleneimine (PEI), zeta potential measurements indicate that EUAC with 10 wt% PEI exhibits a positive charge, enhancing its suitability for adsorbing anionic dyes. The mechanism of methyl orange (MO) adsorption primarily involves heterogeneous multilayer physisorption coupled with electrostatic interactions, facilitated by the modified positive charge on the 10% wt PEI/EUAC, which targets MO as an anionic dye. This finding demonstrated an outstanding MO adsorption ability compared to other studies, as shown in Table 5.

3.5 Reusability

In practical applications, the reusability of the adsorbent has a significant impact on production costs and the environment. This experiment used 10% wt PEI/EUAC and 150 ppm MO as in a ratio of 10 mg : 40 mL. The spent 10% wt PEI/EUAC was also regenerated via rinsing with deionized water, followed by centrifugation at 4500 rpm for 10 min three times, and drying in an oven at 55 °C for 2 hours before testing. The results showed that the MO removal efficiency did not significantly decrease during the five consecutive cycles, as shown in Fig. 10. The first cycle exhibited an MO removal efficiency of 58.8%, which

Table 5 Methyl orange adsorption capacity compared to other studies

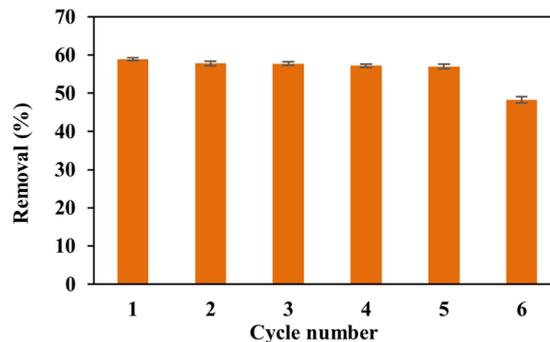| Materials	MO adsorption capacity (mg g^{-1})	Ref.
Spent tea leaves modified with PEI	62.1	22
Fe$_2$O$_3$–biochar nanocomposite	20.5	37
TiO$_2$/sewage sludge AC	7.9	38
Fly ash	67.9	39
Commercial AC	77.1	40
Chitosan/rectorite/CNT composite	50.8	41
10% wt PEI/EUAC	141.7	This work

Fig. 10 Reusability study for the MO adsorption (150 ppm) by 10% wt PEI/EUAC.

slightly decreased to 57.0% in the fifth cycle and dropped to 48.3% at the sixth cycle. These results illustrate that 10% wt PEI/EUAC is a low-cost material with good reusability for MO removal in aqueous solution for at least five cycles.

3.6 Electrochemical properties

Ag/AgCl, Pt wire, and the sample were used as the reference, counter, and working electrodes in a simple three-electrode configuration, using 2 M H$_2$SO$_4$ electrolyte. The CV curves were recorded at the applied potentials of −0.3 to 0.7 V and scan rates of 10 to 40 mV s^{-1}. Fig. 11a shows the CV curves of EUBC, EUAC and 10% wt PEI/EUAC at 30 mV s^{-1}, which displayed a rectangular shape, representing electrical double-layer capacitance (EDLC). Fig. 11b shows the GCD at 1 A g^{-1}. The specific capacitances were calculated via GCD using the following equation.

$$C_p = \left(\frac{I_m \Delta t}{\Delta V} \right) \quad (10)$$

where C_p is the specific capacitance (F g^{-1}), I_m is the current density (A g^{-1}), ΔV is the applied potential window and Δt is the discharging time. The calculated specific capacitances of EUBC, EUAC and 10% wt PEI/EUAC are 39.56 ± 1.56, 263.22 ± 3.77 and 244.30 ± 1.80 F g^{-1}, respectively, at a current density of 1 A g^{-1}, as shown in Fig. 11c.

The energy density (E, W h kg^{-1}) and power density (P, W kg^{-1}) were calculated:

$$E = \left(\frac{C_p \Delta V^2}{2} \right) \quad (11)$$

$$P = \left(\frac{E \times 3.6}{\Delta t} \right) \quad (12)$$

where ΔV and Δt are the potential window and discharge time (s), respectively. The calculated E values of EUBC, EUAC and 10% wt PEI/EUAC are 0.79, 6.48 and 5.76 W h kg^{-1}, respectively (Fig. 12). The calculated P values of EUBC, EUAC and 10% wt PEI/EUAC are 518.53, 542.82 and 538.37 W kg^{-1}, respectively (Fig. 12).

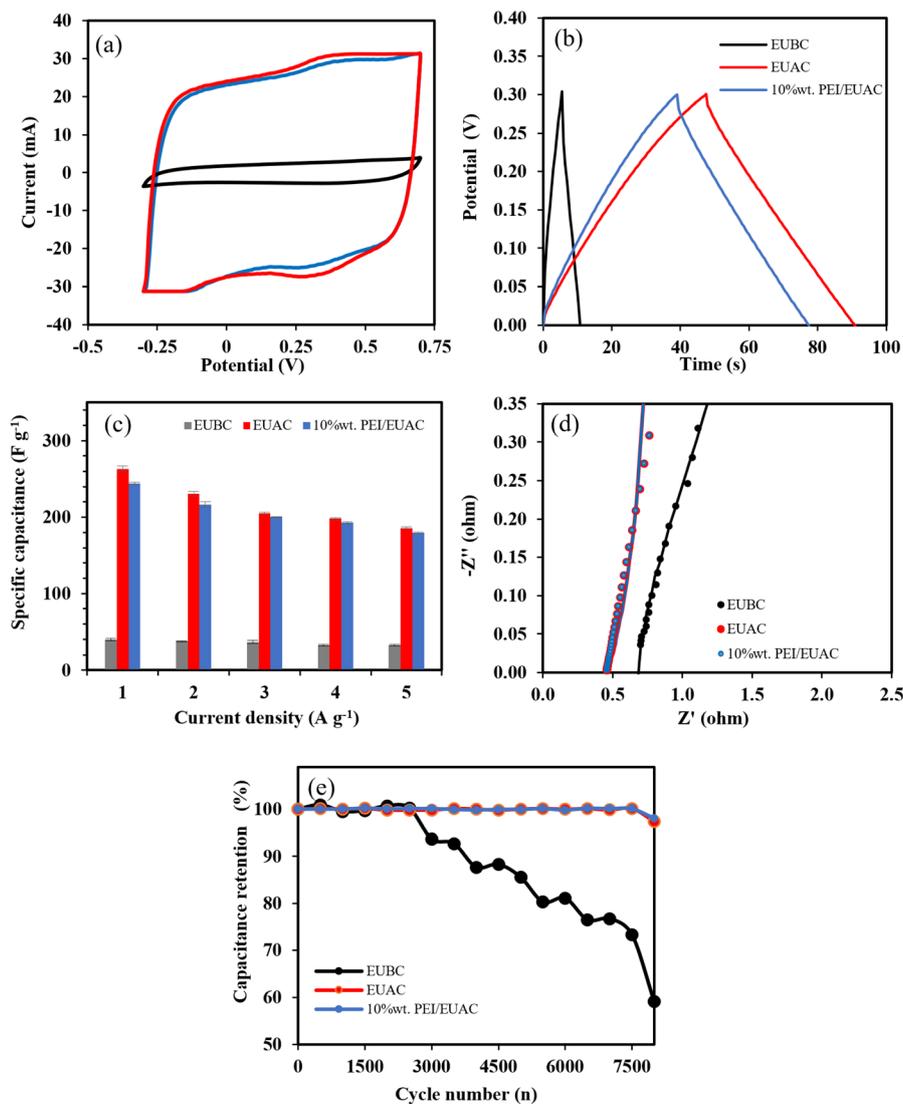Furthermore, EIS is used to assess the characteristics of the electrodes, including conductivity, charge-transfer

Paper

Fig. 11 Electrochemical measurements of EUBC, EUAC and 10% wt PEI/EUAC samples in 2 M H_2SO_4 electrolyte: (a) CV curves at a scan rate of 30 mV s^{-1}, (b) GCD curves at a current density of 1 A g^{-1}, (c) specific capacitances of materials at different current densities, (d) Nyquist plots, and (e) capacitance retention.
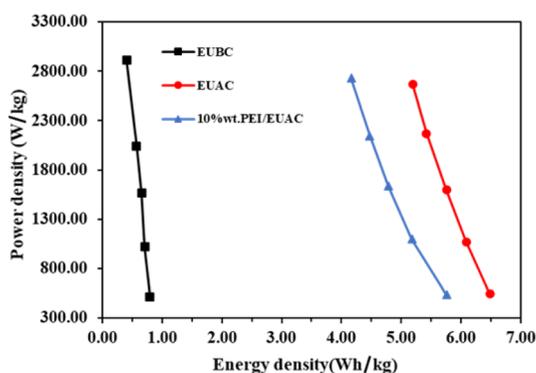

Fig. 12 Ragone plots of EUBC, EUAC and 10% wt PEI/EUAC.

capabilities, and diffusion qualities. Fig. 11d shows the Nyquist plots of EUBC, EUAC and 10% wt PEI/EUAC (10 kHz to 1 Hz); these exhibit two segments comprised of a low-

frequency inclined line and a high-frequency semicircle. The total internal resistance (R_s) values for EUBC, EUAC and 10% wt PEI/EUAC are 0.74, 0.45 and 0.43 ohm respectively. According to the results, the lower specific capacity of EUBC resulted from high internal resistance (R_s) due to a low specific surface. In the case of 10% wt PEI/EUAC, the slightly lower R_s is due to the modified charge from the impregnation with PEI, as confirmed by the zeta potential. Moreover, the cycling stability of electrodes was tested in the potential window of −0.3 to 0.3 V and at 1 A g^{-1}. The retention rates at 8000 cycles for EUBC, EUAC and 10% wt PEI/EUAC were 59.04, 97.35 and 98.07% respectively (Fig. 11e). The significant drop in EUBC's performance is attributed to the material's limited surface area and pore structure, which led to a heterogeneous mixture with the polymer binder. As a result, the coating did not adhere effectively to the current collector, compromising the electrode's stability during the stability test.

4 Conclusions

This study examines the effect of impregnating eucalyptus-derived activated carbon (EUAC) with 10% wt polyethyleneimine (PEI). Introducing 9.39% nitrogen due to PEI doping significantly boosted the methyl orange removal efficiency to 94.43% and maintained the dye removal efficiency over multiple cycles, with a minor drop after the sixth cycle. However, the surface area and pore morphology have not significantly changed after impregnation. The adsorption process adhered to the Sips model and Elovich kinetics, suggesting heterogeneous adsorption, physisorption, and electrostatic adsorption. In the electrochemical test, PEI-treated activated carbon exhibited a remarkable increase in specific capacitance to 244.30 ± 1.80 F g^{-1} with a high retention rate of 98.07% after 8000 cycles. These results highlight the potential of low-cost eucalyptus-derived activated carbon to further contribute to sustainable development goals, especially in providing clean water and affordable energy, leveraging local community involvement for broader economic and environmental benefits.

Data availability

Data will be made available on request.

Author contributions

Conceptualization, T. S.; formal analysis, B. W.; investigation, B. W., T. C., N. P. and T. S.; resources, T. S. and B. W.; writing, original draft, B. W. and T. S.; writing, review & editing, T. C., N. P. and T. S.; visualization, T. S.; supervision, T. S.; funding acquisition, T. S. All authors have read and agreed to the published version of the manuscript.

Conflicts of interest

There are no conflicts to declare.

Acknowledgements

Notes and references

1 W. J. Cosgrove and D. P. Loucks, *Water Resour. Res.*, 2015, **51**, 4823–4839.
2 H. Y. Zhu, Y. Q. Fu, R. Jiang, J. H. Jiang, L. Xiao, G. M. Zeng, S. L. Zhao and Y. Wang, *Chem. Eng. J.*, 2011, **173**, 494–502.
3 A. Deb, S. Das and A. Debnath, *Chem. Phys. Lett.*, 2023, **830**, 140820.
4 B. Saha, A. Debnath and B. Saha, *J. Indian Chem. Soc.*, 2022, **99**, 100635.
5 S. K. Dutta, M. K. Amin, J. Ahmed, M. Elias and M. Mahiuddin, *S. Afr. J. Chem. Eng.*, 2022, **40**, 195–208.
6 L. Asadi Kafshgari, M. Ghorbani and A. Azizi, *Appl. Surf. Sci.*, 2017, **419**, 70–83.
7 J. Fu, Q. Xin, X. Wu, Z. Chen, Y. Yan, S. Liu, M. Wang and Q. Xu, *J. Colloid Interface Sci.*, 2016, **461**, 292–304.
8 Z. Tang, Y. Miao, J. Zhao, H. Xiao, M. Zhang, K. Liu, X. Zhang, L. Huang, L. Chen and H. Wu, *Cellulose*, 2021, **28**, 1527–1540.
9 K. Vikrant, K. H. Kim, Y. S. Ok, D. C. W. Tsang, Y. F. Tsang, B. S. Giri and R. S. Singh, *Sci. Total Environ.*, 2018, **616–617**, 1242–1260.
10 S. Jha, R. Gaur, S. Shahabuddin and I. Tyagi, *Toxics*, 2023, **11**, 117.
11 X. Wang, J. Feng, Y. Cai, M. Fang, M. Kong, A. Alsaedi, T. Hayat and X. Tan, *Sci. Total Environ.*, 2020, **708**, 134575.
12 J. Yu, X. Zhang, D. Wang and P. Li, *Water Sci. Technol.*, 2018, **77**, 1303–1312.
13 D. Laird, P. Fleming, B. Wang, R. Horton and D. Karlen, *Geoderma*, 2010, **158**, 436–442.
14 I. Anastopoulos, M. J. Ahmed and E. H. Hummadi, *J. Mol. Liq.*, 2022, **356**, 118864.
15 S. S. Shafqat, S. H. Sumrra, M. N. Zafar, S. Aslam, M. I. Vohra, M. Nosheen, A. A. Almehizia, S. R. Shafqat and M. A. Khan, *Mater. Today Commun.*, 2024, **39**, 108934.
16 U. Ghani, W. Jiang, K. Hina, A. Idrees, M. Iqbal, M. Ibrahim, R. Saeed, M. K. Irshad and I. Aslam, *Front. Environ. Sci.*, 2022, **10**, DOI: 10.3389/fenvs.2022.887425.
17 X. Xu, Y. Zheng, B. Gao and X. Cao, *Chem. Eng. J.*, 2019, **368**, 564–572.
18 B. Huang, Y. Liu, B. Li, H. Wang and G. Zeng, *RSC Adv.*, 2019, **9**, 32462–32471.
19 Z. Wu, X. Wang, J. Yao, S. Zhan, H. Li, J. Zhang and Z. Qiu, *Sep. Purif. Technol.*, 2021, **277**, 119474.
20 A. H. Nordin, S. Wong, N. Ngadi, M. Mohammad Zainol, N. A. F. Abd Latif and W. Nabgan, *J. Environ. Chem. Eng.*, 2021, **9**, 104639.
21 Y. Liu, S. Wang, H. Zhou, X. Li, L. Duan, S. Chen, S. Li, L. Zhang and A. Zhang, *BioResources*, 2020, **15**, 7342–7356.
22 S. Wong, H. H Tumari, N. Ngadi, N. B. Mohamed, O. Hassan, R. Mat and N. A. Saidina Amin, *J. Cleaner Prod.*, 2019, **206**, 394–406.
23 N. B. Mohamed, N. Ngadi, N. S. Lani and R. Rahman, *Chem. Eng. Trans.*, 2017, **56**, 103–108.
24 B. Üstün, H. Aydın, S. N. Koç, A. Uluslu and Ü. Kurtan, *J. Energy Storage*, 2023, **73**, 108970.
25 S. Zhang, X. Shi, R. Wrąsbel, X. Chen and E. Mijowska, *Electrochim. Acta*, 2019, **294**, 183–191.
26 H. Marsh and F. Reinoso, *Activated Carbon*, Elsevier Science, 2006.
27 E. Bottani and J. Tascón, *Adsorption by Carbons*, Elsevier Science, 2011.
28 T. Li, Z. Tong, B. Gao, Y. C. Li, A. Smyth and H. K. Bayabil, *Environ. Sci. Pollut. Res.*, 2020, **27**, 7420–7429.
29 L. Fu, G. Zhang, S. Wang, L. Zhang and J. Peng, *Appl. Water Sci.*, 2017, **7**, 4247–4254.
30 D. Qu, Z. Sun, M. Zheng, J. Li, Y. Zhang, G. Zhang, H. Zhao, X. Liu and Z. Xie, *Adv. Opt. Mater.*, 2015, **3**, 360–367.

31 X. Zhang, D. Lin and W. Chen, *RSC Adv.*, 2015, **5**, 45136–45143.

32 T. Kato, Y. Yamada, Y. Nishikawa, T. Otomo, H. Sato and S. Sato, *J. Mater. Sci.*, 2021, **56**, 15798–15811.

33 G. S. dos Reis, G. L. Dotto, J. Vieillard, M. L. Oliveira, S. F. Lütke, A. Grimm, L. F. Silva, É. C. Lima, M. Naushad and U. Lassi, *J. Alloys Compd.*, 2023, **960**, 170530.

34 G. S. dos Reis, J. Thivet, E. Laisné, V. Srivastava, A. Grimm, E. C. Lima, D. Bergna, T. Hu, M. Naushad and U. Lassi, *Chem. Eng. Sci.*, 2023, **281**, 119129.

35 G. S. dos Reis, D. Pinto, É. C. Lima, S. Knani, A. Grimm, L. F. Silva, T. R. Cadaval Jr and G. L. Dotto, *React. Funct. Polym.*, 2022, **180**, 105395.

36 T. Phonlam, B. Weerasuk, P. Sataman, T. Duangmanee, S. Thongphanit, K. Nilgumhang, S. Anantachaisilp, T. Chutimasakul, T. Kwamman and V. Chobpattana, *S. Afr. J. Chem. Eng.*, 2023, **43**, 67–78.

37 N. Chaukura, E. C. Murimba and W. Gwenzi, *Appl. Water Sci.*, 2017, **7**, 2175–2186.

38 M. N. Rashed, M. Eltaher and A. Abdou, *R. Soc. Open Sci.*, 2017, **4**, 170834.

39 M. Gao, Q. Ma, Q. Lin, J. Chang, W. Bao and H. Ma, *Appl. Surf. Sci.*, 2015, **359**, 323–330.

40 B. K. Martini, T. G. Daniel, M. Z. Corazza and A. E. de Carvalho, *J. Environ. Chem. Eng.*, 2018, **6**, 6669–6679.

41 J. Chen, X. Shi, Y. Zhan, X. Qiu, Y. Du and H. Deng, *Appl. Surf. Sci.*, 2017, **397**, 133–143.